Clim. Past, 13, 649–665, 2017
https://doi.org/10.5194/cp-13-649-2017

Climate of the Past
Open Access
EGU

Southern Hemisphere anticyclonic circulation drives oceanic and climatic conditions in late Holocene southernmost Africa

Annette Hahn[1], Enno Schefuß[1], Sergio Andò[2], Hayley C. Cawthra[3,4], Peter Frenzel[5], Martin Kugel[1], Stephanie Meschner[5], Gesine Mollenhauer[6], and Matthias Zabel[1]

[1]MARUM – Center for Marine Environmental Sciences, University of Bremen, Bremen, Germany
[2]Department of Earth and Environmental Sciences, University of Milano-Bicocca, Milan, Italy
[3]Geophysics Competency, Council for Geoscience, Cape Town, South Africa
[4]Centre for Coastal Palaeoscience, Nelson Mandela Metropolitan University, Port Elizabeth, South Africa
[5]Institute of Earth Sciences, Friedrich Schiller University of Jena, Jena, Germany
[6]Alfred Wegener Institute, Bremerhaven, Germany

Correspondence to: Annette Hahn (ahahn@marum.de)

Received: 5 October 2016 – Discussion started: 3 November 2016
Revised: 25 April 2017 – Accepted: 2 May 2017 – Published: 9 June 2017

Abstract. Due to the high sensitivity of southern Africa to climate change, a reliable understanding of its hydrological system is crucial. Recent studies of the regional climatic system have revealed a highly complex interplay of forcing factors on precipitation regimes. This includes the influence of the tropical easterlies, the strength of the southern hemispheric westerlies as well as sea surface temperatures along the coast of the subcontinent. However, very few marine records have been available in order to study the coupling of marine and atmospheric circulation systems. Here we present results from a marine sediment core, recovered in shallow waters off the Gouritz River mouth on the south coast of South Africa. Core GeoB18308-1 allows a closer view of the last ∼4 kyr. Climate sensitive organic proxies, like the distribution and isotopic composition of plant-wax lipids as well as indicators for sea surface temperatures and soil input, give information on oceanographic and hydrologic changes during the recorded time period. Moreover, the micropaleontology, mineralogical and elemental composition of the sediments reflect the variability of the terrigenous input to the core site. The combination of down-core sediment signatures and a catchment-wide provenance study indicate that the Little Ice Age (∼ 300–650 cal yr BP) was characterized by climatic conditions favorable to torrential flood events. The Medieval Climate Anomaly (∼ 950–650 cal yr BP) is expressed by lower sea surface temperatures in the Mossel Bay area and humid conditions in the Gouritz River catchment. These new results suggest that the coincidence of humid conditions and cooler sea surface temperatures along the south coast of South Africa resulted from a strengthened and more southerly anticyclonic circulation. Most probably, the transport of moisture from the Indian Ocean by strong subtropical easterlies was coupled with Agulhas Bank upwelling pulses, which were initiated by an increase in Agulhas Current strength.

1 Introduction

South Africa's regional climate has been discerned as particularly sensitive to future climate change. Over the last five decades mean annual temperatures have increased by at least 1.5 times the observed global average and both extreme rainfall events and droughts are anticipated as environmental, social and economic threats (Niang et al., 2014; Ziervogel et al., 2014). It is well known that the precipitation patterns in South Africa are influenced by shifts of the southern hemispheric westerlies (SHW), the strength of the tropical easterlies, as well as variations in ocean circulation (e.g., Chase and Meadows, 2007; Chase et al., 2011; Marzin and Braconnot, 2009; Schefuß et al., 2011; Fig. 1). The interplay and regional extent of these factors and their relation to global climate forcings at different timescales is, however, far from being understood. The main dispute currently concerns the

driving factors behind the easterly rainfall regimes in the southernmost part of Africa (south of ∼ 13–14° S), which is not influenced by modern Intertropical Convergence Zone shifts. A major question in this area is whether the climate variability is synchronous with northern hemispheric variations or driven by direct insolation changes and thus antiphased to northern hemispheric signals. In the past, it was relatively uncontroversial that long term (glacial-interglacial timescale) climate variations in southernmost Africa are directly forced by local insolation (Daniau et al., 2013; Simon et al., 2015). However, recently several paleorecords have emerged showing either no evidence of direct insolation as a climatic driver (Chase et al., 2009, 2010; Dupont et al., 2011) or evidence for opposing trends (i.e., synchrony with the Northern Hemisphere) (Tierney et al., 2008; Stager et al., 2012; Truc et al., 2013). Furthermore, on shorter timescales, recent datasets reveal strong indications for a highly complex local climate system. So far, data from Wonderkrater in eastern South Africa (Truc et al., 2013) and regional pollen analyses (Scott et al., 2012) document enhanced and diminished precipitation with respect to the geographical position of the recording archive. Evidence for climate variability in phase with the Northern Hemisphere is delivered by the regional compilation of pollen records published by Chevailier and Chase (2015) as well as by the progressive Holocene aridification in northwestern Namibia (proposed by Chase et al., 2010) and the simultaneous cool and dry period in eastern South Africa (proposed by Holmgren et al., 1999 and Norström et al., 2014). Mechanisms suggested to explain the transmission of the northern hemispheric signal to southern Africa include teleconnections causing a dipole pattern of rainfall between eastern tropical and southern Africa (Norström et al., 2014) as well as sea surface temperature (SST) changes due to ocean circulation variability (Agulhas strength) (Tierney et al., 2008; Stager et al., 2012; Scott et al., 2012; Truc et al., 2013). The latter can be discerned as a major research gap in southernmost South Africa. Due to the strongly erosive Agulhas Current, very few marine records from the Agulhas Bank exist and the influence of SSTs on the regional precipitation patterns therefore remains under dispute. On the one hand, it has been suggested that decreased SSTs on the southwestern coast of South Africa lead to decreasing precipitation in southernmost South Africa (Rouault et al., 2003) and positive SST anomalies along the east coast associated with Agulhas strengthening enhance summer precipitation in the eastern South Africa (Jury et al., 1993; Dupont et al., 2011; Scott et al., 2012). On the other hand, the oxygen isotope composition of marine mollusk shells preserved in Nelson Bay archaeological cave deposits indicates that during periods of wetter conditions over the southern African interior, the Agulhas surface water temperatures were actually lower than during arid periods (Cohen and Tyson, 1995). Based on these data in combination with interannual observations, a conceptual model relating oceanic and atmospheric circulation systems of southern Africa was proposed in 1995 by Cohen and Tyson. This model predicts that during periods of stronger anticyclonic circulation, the increased alongshore winds caused coastal upwelling in the Mossel Bay area whereas the increased Agulhas strength drives upwelling over the east coast shelf edge. The database behind this model is however sparse and a large gap exists for the period between 2400 and 650 yr BP (Tyson and Lindesay, 1992; Cohen and Tyson, 1995). Our multiproxy study on core GeoB18308-1, located on the south coast of South Africa, off the mouth of the Gouritz River, 30 km west of the town Mossel Bay, aims to close this gap. In addition to providing a SST reconstruction for the past ∼ 4 kyr, this record also holds the potential for a high-resolution continental climatic reconstruction. In order to decipher the complexity of the terrigenous climatic signal, sediment provenance and transport processes are studied using catchment material in a source-to-sink approach.

2 Regional setting

2.1 Gouritz River catchment area

The Gouritz River catchment is located within the year-round rainfall zone (YRZ; Fig. 1) and has a mean annual runoff of ca. 488×10^6 m^3 (Le Maitre et al., 2009). Desmet and Cowling (1999) and Le Maitre et al. (2009), however, note that even though observed rainfall patterns in the catchment area show year-round precipitation, most of the area mainly receives rainfall during summer and autumn. Major floods, e.g., in January 1981, March 2003 and in March 2004, caused by extreme rainfall events, are another characteristic of this area (Desmet and Cowling, 1999; Cowling et al., 2004). Despite the relatively small size of the catchment area (45 715 km^2), the altitudinal gradient is steep as the Swartberg Mountains rise abruptly above 2000 m a.s.l. within 100 km of the coast (Le Maitre et al., 2009).

2.2 Vegetation in the study area

Within the study area three dominant vegetation types are described: Fynbos, Succulent Karoo and the Nama Karoo biomes (Mucina and Rutherford, 2006; see map in Fig. 2). The Fynbos biome is characterized as a Mediterranean-type vegetation (Goldblatt and Manning, 2002). It is found especially along the southern and southwestern coast of South Africa and therefore receives most of its rainfall during austral winter. The most dominant photosynthetic pathway reported is C_3 (Vogel et al., 1978). The Succulent Karoo biome is described as being better adapted to arid conditions and higher summer temperatures (Carr et al., 2014). Due to the geographic distribution of vegetation, the Succulent Karoo biome gets most of its rainfall during winter but also receives summer precipitation in the eastern part of the catchment (Rundel et al., 1999). The last vegetation type, Nama Karoo, is described to consist mostly of C_4 grasses and, due to its

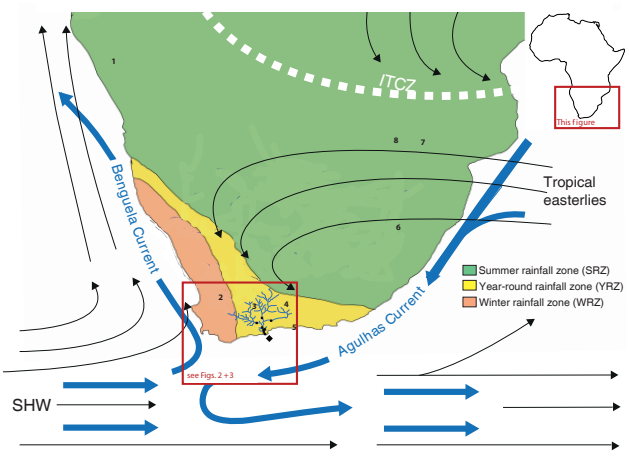

Figure 1. Schematic overview of the main components of the oceanic (thick arrows) and atmospheric (thin arrows) circulation over southern Africa (modified from Truc et al., 2013). The winter rainfall zone is colored in red, the summer rainfall zone in green and the year-round rainfall zone in yellow. Squares indicate localities of Gouritz River samples; diamond indicates marine sediment core location. SHW: southern hemispheric westerlies; ITCZ: Intertropical Convergence Zone. Note that these are shown in their summer position. Austerlitz midden (1), Katbakkies Pass midden (2), Seweweekspoort midden (3), Pinnacle Point (4), Cango Cave (5), Nelson Bay Cave (6), Braamhoek peat (7), Lake Eteza (8), Cold Air Cave (9) and Wonderkrater (10).

occurrence in a northeastern geographical position, receives dominantly summer rain (Le Maitre et al., 2009). Studies within this region as well as in other areas of Africa revealed that these vegetation types showed differences in their *n*-alkane composition (Rommerskirchen et al., 2006; Vogts et al., 2009; Carr, 2012, 2014; Boom et al., 2014; Herrmann et al., 2016; map in Fig. 2).

2.3 Geology of the Gouritz River catchment

The distinctive topography of southern Africa is characterized by a high-relief inland plateau flanked by a low average elevation coastal plain. The Gouritz River catchment drains almost all sequences of the Cape: the Malmesbury Group and the Cape Granite Suite as the oldest "basement" rocks (Rozendaal et al., 1999; Johnson et al., 2006; Milani and de Wit, 2008); the thick siliciclastic sequence of the Cape Supergroup (Thamm and Johnson, 2006; Newton et al., 2006); and the Karoo Supergroup, which was terminated by the extrusion and intrusion of the extensive Drakensberg basalts and dolerites (Duncan et al., 1997). The southern cape continental shelf and the broad, shallow plain, low-relief coastal plain mantled with Pleistocene/Holocene deposits comprise the submerged and emergent portions of a continuous feature (Cawthra et al., 2015). The south coast is characterized by a series of eastward-opening log-spiral bays that extend for approximately 20–40 km between adjacent west–east-trending rocky headlands. The Gouritz River is associated with a well-developed, stratified, sediment wedge (~ 10 km wide and 85 km long) (Birch, 1978) that extends predominantly westwards of the river mouth. Offshore, the Gouritz River is associated with a subdued incised valley, running across the continental shelf (Cawthra, 2014).

2.4 Oceanic circulation on the eastern Agulhas Bank

The oceanography of the Agulhas Bank is strongly influenced by the warm, fast-flowing Agulhas Current originating in the Mozambique Channel (Lutjeharms et al., 2001). The inner shelf targeted in this study is influenced by wind-driven coastal upwelling, particularly during summer (see Hutchings et al., 1995). Along-coast easterly winds drive these periodic events of short-term surface water cooling of up to 8 °C (Schumann et al., 1982; Beckley, 1983). During winter, plumes of warm Agulhas Current water have been observed to advect onto the shelf by southwesterly winds (Lutjeharms and van Ballegooyen, 1988).

3 Material and methods

3.1 Sediment coring and catchment samples

Sediment core GeoB18308-1 was taken with a vibrocorer during RV *METEOR* Cruise M102 in December 2013 from a protected valley fill on the continental shelf near Mossel Bay (34°22.39′ S, 21°55.75′ E) 4 km offshore of the Gouritz River mouth. Using multibeam bathymetry and side-scan sonar Cawthra et al. (2015) describe the morphology of the area as a generally smooth, wide continental shelf of low gradient (see location in Fig. S1 in the Supplement). The core has a total length of 4.94 m and mainly consists of fine sand and mud. In the interval between ~ 30 and 70 cm an event deposit revealing slumped turbidite facies with an erosive contact was identified. South African sea level reconstructions (Compton, 2006; Ramsay and Cooper, 2002) reveal that the sampling site (located in about 40 m water depth) was not significantly influenced by fluctuations during the last 5 kyr. Riverbank, flood deposit and suspension load (obtained by filtering ca. 100 L of water pumped from the rivers' main flow) samples were collected from eight locations along the Gouritz River in March 2015 in order to determine the provenance of the deposited material (see locations in Fig. 2 map).

3.2 Age model

Ages were estimated from nine total organic carbon (TOC) samples, two bivalves, one piece of wood and one crab claw (Table 1). The age model used in this study is based on the radiocarbon ages of non-redeposited material only (Fig. 3). The cleaning procedures as well as the accelerator mass spectrometry (AMS) measurements were carried out in the Poznań Radiocarbon Laboratory, Poland, and Beta Analytic Ra-

Table 1. AMS radiocarbon analyses of bulk TOC and carbonate material from core GeoB18308-1. Depending on sediment type (terrestrial or marine identified using all available data) the Southern Hemisphere calibration curve (SHCal13) (Hogg et al., 2013) or the modeled ocean average curve (Marine13) (Reimer et al., 2013) was used. To the latter a ΔR of 146 ± 85 ^{14}C (Dewar et al., 2012) was applied.

					Cal age yr BP			
Core	Depth (cm)	Lab number	^{14}C age (yr BP)	Material	-2σ	$+2\sigma$	Median	Curve
GeoB18308-1	16.5	Beta-397268	150 ± 30	wood	"post-bomb"	98.2 ± 0.4 pMC		
GeoB18308-1	31	Beta-397269	1560 ± 30	TOC	1384	1240	1466	SHCal13*
GeoB18308-1	60	Poz-61261	670 ± 30	TOC	531	413	640	SHCal13*
GeoB18308-1	69	Beta-397270	1370 ± 30	TOC	1196	1116	1294	SHCal13*
GeoB18308-1	123	Poz-60757	1885 ± 30	crab claw	1503	1103	1293	Marine13*
GeoB18308-1	125	Poz-63976	635 ± 30	TOC	665	553	598	SHCal13
GeoB18308-1	146	Poz-61260	1085 ± 30	wood	1057	934		
	991	SHCal13						
GeoB18308-1	195	Poz-63472	1045 ± 30	TOC	1050	921		
	953	SHCal13						
GeoB18308-1	285	Poz-60754	$10\,100 \pm 50$	bivalve	11 158	10 669	10 920	Marine13*
GeoB18308-1	285	Poz-63585	2075 ± 30	TOC	1689	1292		
	1481	Marine13						
GeoB18308-1	394	Poz-63471	3020 ± 30	TOC	2805	2354		
	2615	Marine13						
GeoB18308-1	408	Poz-63653	2910 ± 30	bivalve	2718	2298	2501	Marine13
GeoB18308-1	440	Poz-63793	3620 ± 30	TOC	3573	3116	3350	Marine13
GeoB18308-1	490	Poz-61290	4180 ± 35	TOC	4341	3816	4058	Marine13

* Redeposited material – not included in age model.

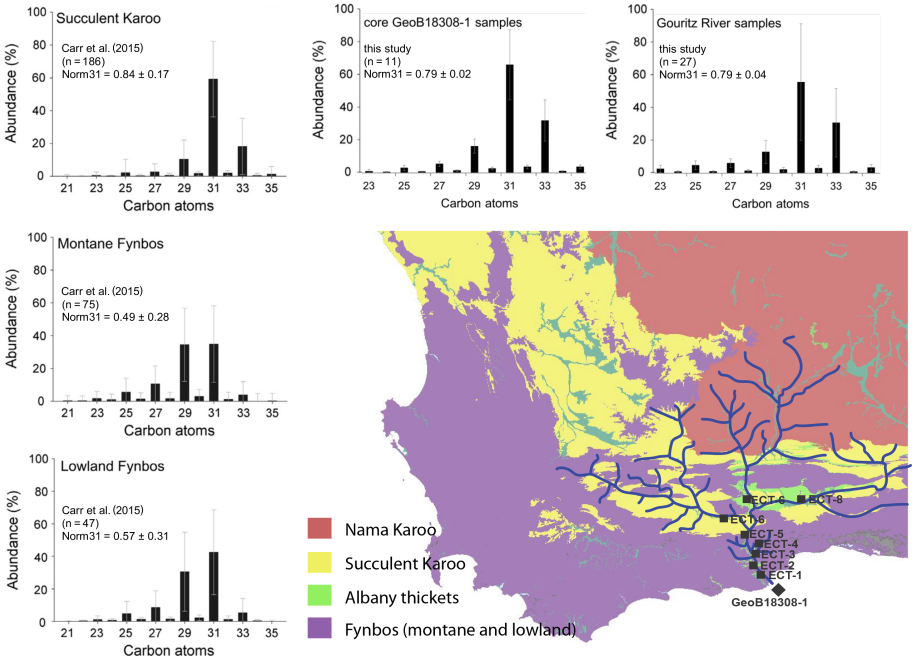

Figure 2. The map is an enlargement of Fig. 1 and shows vegetation types in and around the drainage basin (after Mucina and Rutherford, 2006 and Scott et al., 2012) of the Gouritz River. Squares indicate localities of Gouritz River samples; diamond indicates marine sediment core location. Plots showing regional biome/ecoregion soil and vegetation average *n*-alkane distributions from Carr et al. (2015) are indicated on the left, whereas average *n*-alkane distributions of riverine and marine samples from this study are plotted above the map.

diocarbon Dating Laboratory Florida, USA. Depending on sediment type (terrestrial or marine identified using all available data) either the Southern Hemisphere calibration curve (SHCal13) (Hogg et al., 2013) or the modeled ocean average curve (Marine13) (Reimer et al., 2013) were used to calibrate the radiocarbon ages. The marine ΔR is assumed to be close to the south west coast ΔR (146 ± 85 ^{14}C years) published in 2012 by Dewar et al. (Mike Meadows, personal communication, 2017). The software Bacon (Blaauw and Christen, 2011) was used to calculate an age model. We refer to median age estimations in this paper; please note the associated uncertainty indicated in Fig. 3 and Table 1.

3.3 Inorganic geochemistry

Inorganic geochemical analyses were performed down-core (2 to 10 cm resolution) as well as on soil, riverbank, flood deposit and suspension load samples collected from eight Gouritz catchment locations (ECT-1 to ECT-8) in March 2015 (Fig. 2, Table 2). Elemental profiles were collected using MARUM XRF Core Scanner II (AVAATECH serial no. 2) equipped with an Oxford Instruments 50W XTF5011 rhodium X-ray tube, a Canberra X-PIPS silicon drift detector (SDD; model SXD 15C-150-500) run at a 150 eV resolution and a Canberra digital spectrum analyzer (DAS 1000) at the MARUM – University of Bremen. The vertical resolution was 1 cm with two generator settings (30 kV, 1 mA, 20 s; 10 kV, 0.2 kV, 20 s) for detection of different elemental groups. For calibration purposes the XRF-spectrometer measurements were completed on 28 selected dried and ground sediment samples using a PANalytical Epsilon3-XL XRF spectrometer (methodology in Govin et al., 2014). Using these discrete ED-XRF measurements and the procedure proposed by Lyle et al. (2012) we were able to normalize the XRF scanning data (counts). Good correlations (R^2 above 0.7) of XRF scanner and XRF analyses of discrete samples results were found for a variety of elements including Ca and Fe.

3.4 Organic geochemistry

The continuous high-resolution, XRF scanning dataset (Fig. S2) indicates little variability in the lower half of core GeoB18308-1. Based on this finding subsamples for biomarker analysis were taken at higher resolution in the upper half of the core.

3.4.1 Plant-wax analyses

Dried and ground samples were extracted using a DIONEX accelerated solvent extractor (ASE 200) at 100 °C, 1000 psi with a 9 : 1 mixture of dichloromethane (DCM) to methanol for 5 min and three extraction cycles. Prior to extraction, squalane and C_{46}-GDGT (glycerol dialkyl glycerol tetraether) were added as internal standards. Asphaltenes

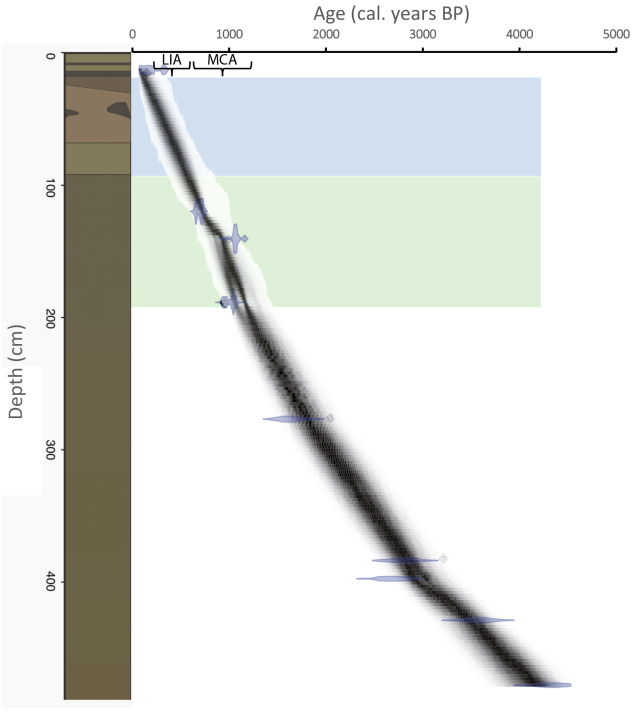

Figure 3. Left: core log of GeoB18308-1 (internal structures with recorded colors) demonstrating the presence of an event deposit (blue box). Right: the calibrated ^{14}C dates (transparent blue) and the age–depth model (darker greys indicate more likely calendar ages; grey stippled lines show 95 % confidence intervals; red curve shows single "best" model based on the weighed mean age for each depth). The green box marks horizons of increased terrestrial input where a terrestrial calibration curve (SHCal13: Southern Hemisphere; Hogg et al., 2013) was used. Otherwise, Marine13-modeled ocean average (Reimer et al., 2013) with a δR following Dewar et al. (2012). Redeposited material (i.e., a crab claw at 123 cm depth, a bivalve at 285 cm and the reworked package at 30–60 cm depth) were excluded from the age–depth modeling. Medieval Climate Anomaly (MCA) and the Little Ice Age (LIA) are indicated.

were removed from the total lipid extracts using Na_2SO_4 columns and elution with hexane. Extracts were saponified for 2 h at 85 °C in 500 µL of a 0.1 M KOH solution in methanol (MeOH). Neutral lipids were recovered by liquid–liquid extraction using hexane. Lipid fractions were separated over a silica gel column (10 % deactivated) using hexane (hydrocarbons), DCM (ketones), and DCM : MeOH 1 : 1 (polar fractions). Unsaturated compounds were removed from the hydrocarbon fractions by column chromatography over $AgNO_3$-coated silica using hexane. The saturated hydrocarbon fractions containing *n*-alkanes were injected in splitless mode at 260 °C into a Thermo Scientific Focus gas chromatograph equipped with a DB-5ms column (30 m × 0.25 mm, 0.25 µm film thickness, Agilent Technologies, Palo Alto, USA) coupled to a flame ionization detector (GC-FID). The oven was held at 70 °C for 2 min, then heated at a rate of 20 °C min^{-1} to 150 °C, and after with a rate of 4 °C min^{-1}

Table 2. *n*-Alkane isotopic composition and distribution descriptive parameters averaged (with standard deviation).

Sample name	Latitude (decimal degrees)	Longitude	$\delta^{13}C_{C_{31}}$ ‰ VPDB	Standard deviation $\delta^{13}C_{C_{31}}$	$\delta D_{C_{31}}$ ‰ VSMOW	Standard deviation $\delta D_{C_{31}}$	Norm31	Sample material
ECT-1-2	−34.28081	21.82842	−26.77	0.05	−127.29	2.69	0.85	soil horizon
ECT-1-3	−34.28081	21.82842	−29.10	0.10	−136.96	0.43	0.83	paleoflood deposit
ECT-2-1	−34.18470	21.75288	−28.84	0.05	−127.30	0.22	0.76	paleoflood deposit
ECT-3-1a	−34.08183	21.74178	−27.92	0.21	−129.86	0.92	0.78	soil horizon
ECT-3-1b	−34.08183	21.74178	−27.74	0.07	−139.18	0.83	0.73	paleoflood deposit
ECT-5-1	−33.90890	21.65330	−29.50	0.08	−130.13	0.13	0.78	soil horizon
ECT-5-2	−33.90890	21.65330	−29.44	0.15	−132.31	0.23	0.81	paleoflood deposit
ECT-6-1	−33.90917	21.65353	−29.14	0.05	−134.38	1.09	0.83	paleoflood deposit
ECT-6-2	−33.90917	21.65353	−28.14	0.10	−128.87	0.09	0.82	soil horizon
ECT-7-2	−33.75837	21.46945	−29.66	0.08	−131.94	1.35	0.74	riverbank deposit
ECT-8-1	−33.62422	22.22843	−31.56	0.06	−128.20	0.23	0.77	riverbank deposit

to 320 °C, and remained at this temperature for 16.5 min. An external calibration standard containing *n*-alkanes of known concentrations was analyzed every six samples. Based on the repeated standard analyses, the precision of quantification is calculated to 5 %. The ratio between C_{29} and C_{31} *n*-alkanes (Norm31) was calculated using Eq. (1):

$$\text{Norm31} = C_{31}/(C_{29} + C_{31}). \quad (1)$$

The carbon preference index (CPI) (Bray and Evans, 1961) was calculated according to Eq. (1):

$$\text{CPI}_{23-33} = \frac{1}{2}\left\{\left(\frac{C_{23}+C_{25}+C_{27}+C_{29}+C_{31}+C_{33}}{C_{22}+C_{24}+C_{26}+C_{28}+C_{30}+C_{32}}\right) + \left(\frac{C_{23}+C_{25}+C_{27}+C_{29}+C_{31}+C_{33}}{C_{24}+C_{26}+C_{28}+C_{30}+C_{32}+C_{34}}\right)\right\}. \quad (2)$$

3.4.2 Compound-specific carbon and hydrogen isotope analyses

The fractions containing *n*-alkanes were used for compound-specific carbon and hydrogen isotope analyses. Compound-specific stable hydrogen isotope measurements were performed on a Trace GC (Thermo Fisher Scientific, Bremen, Germany) coupled to a MAT 253 IRMS (Finnigan MAT, Bremen, Germany) via a pyrolysis reactor operated at 1420 °C. The PTV injector was maintained at 45 °C at injection and then heated to 340 °C to transfer the sample onto the GC column. Compounds were separated on a Rxi-5ms silica column (30 m × 0.25 mm, 0.25 µm film thickness, Restek, Bellefonte, USA). The GC was maintained at 120 °C for 3 min then heated to 200 °C with 30 °C min^{-1}, then at 4 °C min^{-1} to 320 °C and held for 24 min. H_2 reference gas was used for isotope calibration. The δD values are expressed in per mill relative to VSMOW. The H3+ factor varied around 6.12 ± 0.02 ppm nA^{-1}. Long-term repeated analysis of the external standard mixture with 16 *n*-alkanes rendered a precision (1σ) of ±3 ‰ and an average accuracy of 0 ‰. The internal standard squalene had an accuracy and precision of 0 and 2 ‰, respectively.

Carbon isotope compositions of the *n*-alkanes were analyzed on the same type of GC coupled to a MAT 252 IRMS via a modified GC/C III combustion interface operated at 1000 °C. Injector and GC setting were similar to that for δD analysis. Calibrated CO_2 reference gas was used for isotope calibration. Values are expressed in δ^{13}C relative to VPDB. Long-term repeated analysis of the external standard mixture with 16 *n*-alkanes rendered a precision (1σ) of ±0.3 ‰ and an average accuracy of 0.4 ‰. The internal standard squalene had an accuracy and precision of 0.4 and 0.2 ‰, respectively.

3.4.3 Analysis of GDGTs

The concentrations of glycerol dibiphytanyl glycerol tetraethers (GDGTs) were determined at the Department of Geoscience, University of Bremen. Polar fractions containing GDGTs were filtered through a 0.45 µm PTFE filter and weighed before analysis. The instrument used to determine GDGT concentrations was an Agilent 1200 series high-performance liquid chromatograph (HPLC) coupled with an atmospheric pressure chemical ionization interface (APCI) to an Agilent 6120 quadrupole mass spectrometer (MS). A detailed description of the method this is based on can be found in, for example, Hopmans et al. (2000). GDGTs were eluted over a Prevail Cyano column (Grace, 3 µm, 150 mm × 2.1 mm) maintained at 30 °C using a gradient of solvent A (*n*-hexane) and B (5 % isopropanol in *n*-hexane) from 80 % solvent A (5 min) followed by a linear increase to 36 % solvent B in 40 min. The flow rate was 0.2 mL min^{-1}. GDGTs were detected in positive-ion mode of the APCI-MS and selective ion monitoring (SIM). The APCI spray-chamber specifications were as follows: nebulizer pressure 50 psi, vaporizer temperature 350 °C, N_2 drying gas flow 5 L min^{-1} and 350 °C, capillary voltage −4 kV and corona current +5 µA. Peak areas of the target compounds were used to compute

the following proxies. The TetraEther indeX TEX_{86}^{H} was used as a proxy to estimate SSTs (Kim et al., 2010). The TEX_{86}^{H} is based on the ratio between isoprenoidal GDGTs of 86 carbon atoms, containing one, two and three cyclopentane moieties (I, II and III) as well as the regioisomer of crenarchaeol, a GDGT with 4 cyclopentane moiety (V′). These compounds represent membrane constituents of planktonic archaea, which were found to shift in abundance with changing SSTs (Schouten et al., 2002). TEX_{86}^{H} was calculated with Eq. (2), whereas for SST reconstruction Eq. (4) was used (Kim et al., 2010).

$$TEX_{86^H} = \frac{\log\left[II + III + V'\right]}{[I + II + III + V']} \quad (3)$$

$$SST = 68.4 \times (TEX_{86}^{H}) + 38.6 \quad (4)$$

The branched and isoprenoid tetraether (BIT) (Eq. 5) was derived from the relative abundance of branched glycerol dialkyl glycerol tetraethers (brGDGTs) and the isoprenoid GDGT crenarchaeol (Hopmans et al., 2004). While brGDGTs are thought to be produced by soil bacteria, crenarchaeol is known to be a biomarker for planktonic archaea. Hence, the index is widely used as a proxy for soil input (Weijers et al., 2014, and references therein).

$$BIT = \frac{[I + II + III]}{[I + II + III] + [V]} \quad (5)$$

A relationship between BIT and the tetraether index TEX_{86}^{H} (Fig. S3) is not evident, ruling out a possible alteration of the TEX_{86}^{H} signal near big river flows as indicated by Weijers et al. (2014). Comparison of core-top TEX_{86}^{H}-based SST estimates from GeoB18308-1 with satellite-derived SSTs (MODIS-A ftp://podaac-ftp.jpl.nasa.gov) reveals similar temperatures (Locarini et al., 2013). Reconstructed SST values are therefore assumed to reflect mean annual values.

3.5 Grain size

Particle size distribution was obtained by laser diffraction, using a Malvern Mastersizer 2000 fitted with a Hydro 2000G dispersion unit. Scattered light data were recorded from 2000 to 5000 snapshots of 10 µs. A polydisperse mode of analysis and a refractive index of 1.533 with an adsorption of 0.1 were chosen. Size data collection was performed at constant obscuration in the range 10–20 %. Visible shell fragments were removed prior to measurement.

3.6 Micropaleontology

Microfossils from 16 samples from core GeoB18308-1 were analyzed. The sample volumes vary between 1 and 9 mL around an average of 5 mL and represent a 1 cm thick horizon each. After wet sieving, the > 200 µm size fraction of the dried residues was picked under a low-power stereomicroscope for all ostracods and foraminifers. Other microfossils or fragments of larger forms were counted at group level and only selected specimens of those were picked as a reference. If possible, all taxa were identified to the species level, relying on Benson and Maddocks (1964), Dingle (1992, 1993, 1994), Dingle and Honigstein (1994) Martens et al. (1996) for Ostracoda, and mainly on Lowry (1987) and Schmidt-Sinns (2008) for Foraminifera. Relative abundances (percentages) are calculated for samples with at least 30 specimens to keep a large number for statistical analysis; samples contain about 100 specimens on average. Statistical analysis was carried out using the program package PAST (Hammer et al., 2001). A principal component analysis (PCA) was used for identifying main factors structuring the changing association composition within the core (Fig. S4). Association data are composed of relative abundance data grouping selected species on the genus level if ecologically reliable. Only taxa occurring in at least two samples and with a proportion of more than 5 % in at least one sample are considered. Before running the PCA, a Spearman rank correlation was applied for identifying highly correlating taxa, which was not detected.

3.7 Heavy mineralogy

We have studied the mineralogy of three point-counted samples (from down-core depths of 11 and 285 cm and from catchment sample ECT2-1) at the Laboratory for Provenance Studies, University of Milano-Bicocca. From a quartered aliquot of each bulk sample (5–10 g), sediments were wet sieved with a standard 500 µm sieve in steel and with handmade special tissue net sieves of 15 µm. The fraction > 500 µm and < 15 µm were dried after sieving and weighed for a quantitative estimation of each granulometric class. Heavy minerals were after separated by centrifuging in sodium polytungstate (density 2.90 g cm^{-3}) in the 15–500 µm size window and recovered by partial freezing with liquid nitrogen. Heavy minerals after separation were also weighed. An appropriate amount of heavy minerals was split and mounted with Canada balsam ($n = 1.54$), and 200 to 250 transparent heavy-mineral grains were point-counted at suitable regular spacing (100 µm) under a polarizing microscope to obtain real volume percentages (Galehouse, 1971). During point counting we have also studied surface textures on detrital grains by polarizing microscope to estimate chemical dissolution (Andò et al., 2012). Dubious grains were checked and properly identified by an inVia Renishaw Raman spectrometer equipped with a green laser (532 nm) and a 50 × LWD objective, in the spectral range (144–4000 cm^{-1}) referring to Andò and Garzanti (2013). Heavy-mineral concentration was calculated as the weight percentage of total heavy minerals (HMC) and transparent heavy minerals (tHMC).

4 Results

4.1 On- and offshore samples

4.1.1 Isotope geochemistry

The CPI of all samples ranged from 7.5 to 14.4, indicating generally fresh, hardly degraded material. Down-core as well as in the catchment samples (Fig. 4e, g; Fig. 5; Table 2; Table 3) the average relative contributions of the long-chain *n*-alkanes are *n*-C_{29} ∼ 15–23 %, *n*-C_{31} ∼ 40–50 %, and *n*-C_{33} ∼ 20–24 %. Together, these compounds accounted for 80–90 % of the total *n*-alkanes. The most abundant *n*-alkane is the *n*-C_{31} alkane. Due to the consistent and strong predominance of the *n*-C_{31} alkane further discussion is focused on this compound. $\delta^{13}C$ analyses of the *n*-C_{31} alkane revealed only minor differences (−28.5 to −26.7 ‰ VPDB). The precision is 0.1 ‰ on average with a maximum of 0.3 ‰. Similarly, the Norm31 showed values varying only minimally from 0.75 to 0.82. Larger differences (ranging from −143 to −127 ‰) could be detected in the δD composition of the *n*-C_{31} alkane. Average precision is 1 ‰.

4.1.2 Heavy mineralogy

In the studied samples (Fig. S5), heavy-mineral concentrations in silt and sand fraction (15–500 m) range from very poor (< 0.5 wt % HMC) or poor (0.5 wt % ≤ HMC < 1 wt %) to moderately rich (2 HMC). In Gouritz River catchment sample ECT2-1, clinopyroxenes dominate with subordinate ultrastable zircon, tourmaline, rutile (ZTR), apatite, garnet and titanite; common amphibole; and rare orthopyroxene. The sample, from 11.5 cm depth in core GeoB18308-1, has a very similar heavy-mineral assemblage with slightly lower content of clinopyroxene and more epidote, very rare chloritoid and orthopyroxene. Red flowers of hematite are detected and corrosion features of clinopyroxenes are similar to the Gourtiz River assemblage. The sample, from 285 cm depth in Mossel Bay core GeoB18308-1, is very similar in composition to the Gouritz River but hematite is extremely rare.

4.1.3 Microfossil distribution and PCA results

A diverse foraminifer (at least 46 species) and ostracod (60 species) fauna characteristic for a sublittoral environment was found in the studied core. Beside skeletons of marine invertebrates, continental taxa like plant remains, charophyte oospores, insects, fruits and seeds occur as well, but in low numbers. A continental input is also reflected by six freshwater and four brackish water ostracod taxa occurring in several depths but in rather low numbers. Results of the loading plot analysis of the first principal component show that freshwater ostracods, charophytes, and fruits and seeds coming from continental waters or even of terrestrial origin are associated with high PC1 values. Microfossil results can thus be summarized in an index for estuarian inflow (based on PC1, which is best explained by fluvial input) (Fig. S4).

4.2 Down-core variations

Results of AMS-^{14}C determination are presented in Table 1. The basal age of core GeoB18308-1 is ∼ 4100 cal yr BP (Fig. 3). The continuous high-resolution, XRF scanning dataset (Fig. S2) indicates little variability in the lower half of core GeoB18308-1. However, a time interval of abrupt increase in Fe, clay and silt content (up to 55 %) with more estuarine-inflow-related microfossils (increased PC1), higher BIT (from ∼ 0.06 to 0.81) and enriched δD values of the *n*-C_{31} alkane (up to −127 ‰) can be observed during the period between 950 and 650 cal yr BP (Fig. 4a–c, e–f). These trends are accompanied by a slight depletion in $\delta^{13}C$ of the *n*-C_{31} alkane (up to −28.5 ‰) and to generally lower but highly variable TEX^{H}_{86}-based (from ∼ 0.49 to 0.41) SST values (12.2 to 17.1 °C) (Fig. 4d, g).

5 Discussion

5.1 Catchment samples – source signatures

5.1.1 Linking catchment depositional processes to rainfall regimes

The catchment samples analyzed for plant wax isotopic composition were all taken at lowland locations. However, samples from horizons of darker, finer material identified as soils show distinct $\delta D_{C_{31}}$ differences (∼ 10 ‰ VSMOW) relative to samples identified as flood deposits by their lighter, coarser facies (Fig. 5). As hydrogen used for biosynthesis of plant waxes originates directly from the water taken up by the plants, isotope changes measured in these compounds are related to isotope composition of precipitation (Sessions et al., 1999). This indicates that the plant waxes contained in soil horizons were synthesized under conditions distinct from those under which plants waxes contained in flood deposits were synthesized. δD signatures can also give an indication of the respective conditions; in the Gouritz River catchment the extreme elevation difference is most likely the main influence on rainfall δD signatures which becomes deuterium-depleted with altitude (ca. 10–15 ‰ per 1000 m; Gonfiantini et al., 2001). The relatively deuterium-depleted flood deposits ($\delta D_{C_{31}}$ values of ∼ −138 ‰ vs. ∼ −127 ‰ in soil horizons) indicate that all analyzed flood deposits contain a considerable amount of upper-catchment material. Despite the dominant summer rains in most of the catchment area (Le Maitre et al., 2009), SHW-related precipitation events in the otherwise arid winters have been described as the main precipitation signal influencing the Seweweekspoort record in the upper most Gouritz River catchment by Chase et al. (2013). Since plant material synthesized in the upper part of the catchment characterizes the δD signature of paleoflood deposits sampled in the lowlands, we suggest that

Table 3. GeoB18308-1 organic geochemical down-core data. *n*-Alkane isotopic composition and distribution descriptive parameters averaged (with standard deviation), BIT, TEX_{86}^{H} and SSTs (°C) calculated from TEX_{86}^{H} after Kim et al. (2010).

Depth (cm)	$\delta^{13}C_{C_{31}}$ ‰ VPDB	Standard deviation $\delta^{13}C_{C_{31}}$	$\delta D_{C_{31}}$ ‰ VSMOW	Standard deviation $\delta D_{C_{31}}$	Norm31	BIT	TEX_{86}^{H}	SST(°C) (Kim et al., 2010)
2.5	−28.490	0.284	−134.312	1.978	0.802	0.211	0.477	16.6
12.5	−28.480	0.049	−130.655	0.267	0.790	0.301	0.483	17.0
17.5	−27.630	0.045	−133.604	0.653	0.816	0.701	0.538	20.2
32.5	−27.969	0.168	−136.375	1.441	0.814	0.813	0.593	23.1
52.5	−27.802	0.009	−135.387	1.719	0.820	0.526	0.538	20.2
67.5	−28.063	0.003	−133.719	0.800	0.790	0.732	0.623	24.5
77.5	−28.286	0.026	−129.138	2.394	0.777	0.098	0.477	16.6
107.5	−27.724	0.006	−136.198	0.822	0.789	0.132	0.484	17.1
112.5	−27.446	0.118	−133.986	0.155	0.801	0.306	0.481	16.9
115	−27.449	0.004	−126.742	0.999	0.824	0.193	0.488	17.3
122.5	−27.781	0.295	−131.669	0.458	0.806	0.094	0.409	12.0
130	−27.714	0.040	−127.357	0.338	0.793	0.274	0.447	14.7
142.5	−27.757	0.175	−131.973	0.225	0.800	0.194	0.492	17.5
152.5	−27.696	0.089	−134.566	1.495	0.775	0.101	0.482	16.9
155	−27.461	0.054	−133.870	0.728	0.782	0.224	0.444	14.5
162.5	−27.871	0.046	−136.287	0.535	0.768	0.343	0.524	19.4
165	−26.706	No value	−130.842	1.740	0.775	0.229	0.448	14.8
172.5	−27.323	0.161	−133.485	0.921	0.770	0.156	0.462	15.7
180	−27.454	0.001	−135.430	0.911	0.775	0.313	0.456	15.2
187.5	−27.633	0.149	−136.050	0.655	0.762	0.309	0.496	17.8
207.5	−27.430	0.222	−136.687	No value	0.785	0.063	0.477	16.6
287.5	−27.459	No value	−137.911	2.688	0.803	0.126	0.460	15.6
327.5	−27.475	0.072	−139.901	1.058	0.769	0.117	0.474	16.4
397.5	−27.213	0.027	−141.268	0.301	0.765	0.150	0.463	15.7
452.5	−27.610	0.023	−138.820	1.432	0.781	0.159	0.471	16.2
482.5	−27.626	No value	−142.785	No value	0.754	0.100	0.471	16.3
487.5	−27.181	0.023	−137.367	0.767	0.749	0.087	0.471	16.3

these winterly SHW related precipitation events in the headlands are a main cause for large Gouritz River flood events.

5.1.2 Sediment provenance indicators

Leaf wax *n*-alkane distributions and $\delta^{13}C_{C_{31}}$

Different vegetation types show variations in the *n*-alkane distribution of their leaf waxes. In general, it is thought that plants adapted to higher aridity produce longer-chain wax components than those in habitats of temperate regions (Gagosian and Peltzer, 1986). Therefore, the distribution of *n*-alkane chain length is widely used as an environmental proxy and the *n*-alkane distribution ratio "Norm31" can indicate changes of the source area (Carr et al., 2014). The stable carbon isotopic composition of organic matter reflects the isotopic composition of the carbon source as well as the discrimination between ^{12}C and ^{13}C during biosynthesis (Collister et al., 1994). In particular, compound-specific $\delta^{13}C$ of long-chained *n*-alkanes shows variations with changes in vegetation type (Collister et al., 1994). In this study, the *n*-C_{31} alkane is the most abundant *n*-alkane of the plant waxes and thus used as an indicator of vegetation type in addition to Norm31 ratios. Carr et al. (2014) show vegetation-specific distributions of *n*-alkane homologues within the arid-zone South African flora (Fig. 2). In the case of Gouritz River catchment samples and GeoB18308-1 down-core samples, plant waxes indicate a dominant Karoo vegetation signature according to Carr et al. (2014) and Hermann et al. (2016) (Fig. 2). This vegetation type is dominant in the northern parts of the catchment area (see map in Fig. 2). The flood deposits, soil and suspension load samples analyzed in this study, however, indicate that even in the lower catchment area the Karoo vegetation signature is dominant in the flood as well as in the soil deposits (Table 2, Fig. 2). This may be attributed to (a) difficulties in attributing vegetation types to *n*-alkane distributions caused by crassulacean acid metabolism (CAM) plants existing in South Africa's southernmost vegetation (Boom et al., 2014), (b) the presence of succulent and Karoo plants in areas classified as "Fynbos biome", and (c) an overprint of the lower catchment signature by depositional material originating from the upper catchment. Understanding these processes in detail is

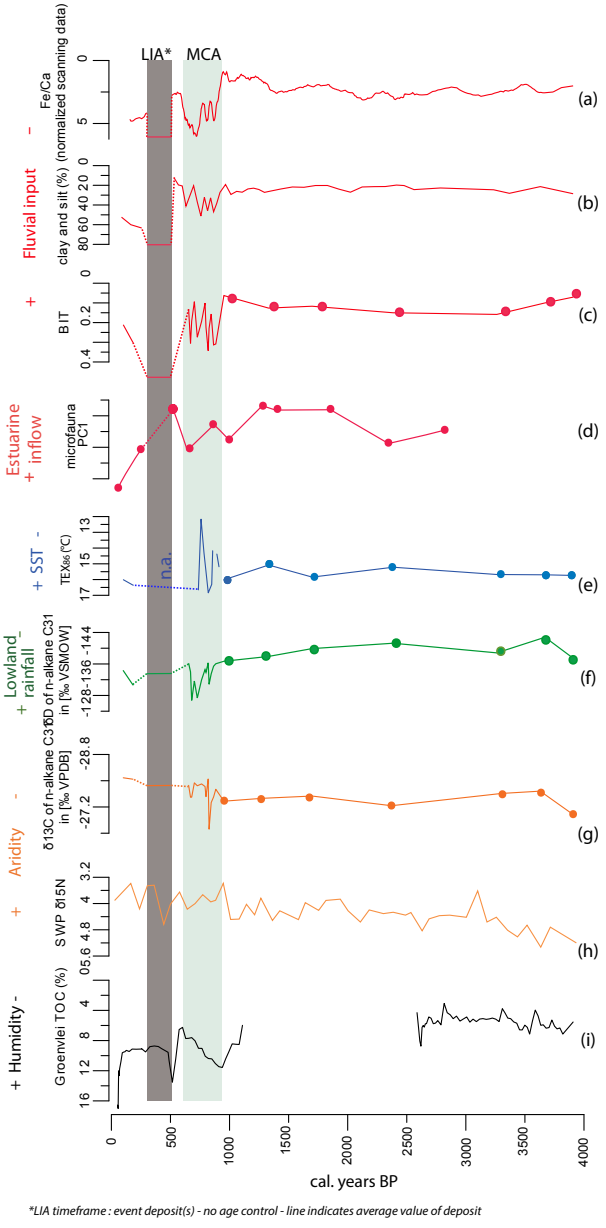

Figure 4. Organic and inorganic down-core geochemistry of GeoB18308-1 **(a–g)** as indicators for fluvial input, SST, SRZ and aridity. Low-resolution records are marked by colored dots. SSTs for samples with BIT above 0.3 were not calculated. The indicator of estuarian inflow is deduced from factor loadings along axes 1 of a PCA on microfossil distribution of core samples. For comparative purposes regional paleoenvironmental records are plotted: **(h)** aridity index from Seweweekspoort (Chase et al., 2013) and **(i)** indirect humidity index from Groenvlei (Wündsch et al., 2016).

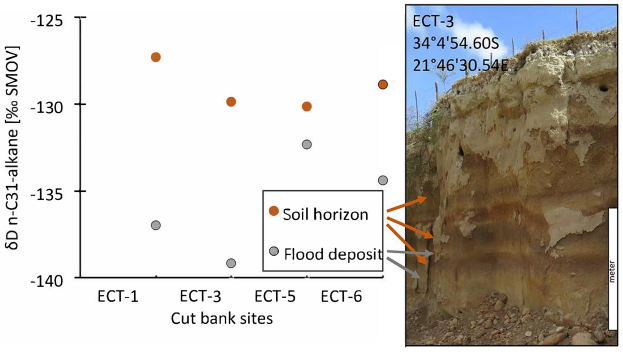

Figure 5. Variations in δD of the n-C_{31}-alkane (‰ VSMOW) in the distinct horizons of paleoflood vs. soil formation horizons. Gouritz River tributary cut bank at sample location ECT-3 is depicted as an example illustrating these alternating horizons.

beyond the scope of this study. Instead, n-alkane distributions and their isotopic values are used as provenance indicators. In the Gouritz River catchment as well as in down-core samples both indicators of vegetation type have similar signatures (identical average Norm31 values of 0.79 and average $\delta^{13}C_{C_{31}}$ of −28.5 and ∼ −26.7 ‰, respectively) and show just minor variations (SD of Norm31 and $\delta^{13}C_{C_3}$ down-core = 0.02 and 0.4, respectively; $n = 27$) (Fig. 2, Table 2). We therefore infer that the sediments deposited at the GeoB18308 site originate directly from the Gouritz River catchment area.

Heavy mineralogy

Heavy-mineral analysis represents an independent powerful tool in provenance studies. In the Gouritz River catchment as well as in samples from GeoB18308-1 clinopyroxenes dominate with subordinate ultrastable zircon, tourmaline, rutile (ZTR), apatite, garnet and titanite, common amphibole and rare orthopyroxene. The significant contribution of ultrastable ZTR to the heavy-mineral assemblages of GeoB18308-1 samples reflects the Gouritz River Cape Supergroup sandstone-dominated geology. The abundance of corroded clinopyroxene indicates weathering of doleritic dikes located only in the uppermost parts of the Gouritz River catchment. Although mineral and organic loads do not necessarily derive from the same source area, when used as provenance indicators both suggest a (upper) Gouritz River catchment provenance for the sediments deposited at the GeoB18308-1 site.

5.2 GeoB18308-1 paleoclimate record

5.2.1 ∼4000–950 cal yr BP – stable arid conditions

The oldest part of the 18308-1 paleorecord (∼4058–950 cal yr BP) is characterized by a relatively low Fe/Ca ratio and a domination of the sand size fraction (mud and silt content below 20–30 %). We associate this with winnowing of fine-grained material by the strong current field inherent to the coastal Agulhas Bank. Heavy-mineral analyses from this part of the core (285 cm) show that hematite is extremely rare, suggesting a dry period without formation of iron oxides

Table 4. Mineralogical composition of heavy minerals in silt and sand fraction (15–500 m) of marine sediments from GeoB18308-1 and Gouritz River catchment.

Location	Sample name	HM %weight	Zircon	Tourmaline	Rutile	Titanite	Apatite	Epidote	Garnet	Chloritoid	Sillimanite	Amphibole	Clinopyroxene	Orthopyroxene	Total	ZTR	% transparent	% opaque	% Fe oxides	% Ti oxides	% turbid HM	Total
Gouritz River: Bland's Drift	ECT2-1	1.5	4	2	1	5	6	9	7	0	0	4	62	1	100	6	67 %	8 %	15 %	9 %	1 %	100 %
Mossel Bay 5 km offshore	GeoB18308-1 (11 cm)	1.3	6	4	5	3	6	19	5	1	0	5	46	2	100	15	72 %	10 %	7 %	11 %	0 %	100 %
Mossel Bay 5 km offshore	GeoB18308-1 (285 cm)	1.3	7	2	2	3	4	10	7	0	0	2	60	2	100	12	77 %	10 %	1 %	12 %	0 %	100 %

in the catchment area. Further afield in South Africa, pollen data from Lake Eteza (South African east coast) reported relative dryness for this period. This was deduced from evidence for decreasing trees and shrubs vegetation accompanied by increasing herbaceous plants (Neumann et al., 2010; Scott et al., 2012). The high-resolution XRF records indicate little variability in the composition of the supplied sediments which is in accordance with the relatively stable conditions recorded in the millennia prior to ∼ 1000 cal yr BP in the speleothem layer width from the Cold Air Cave (Holmgren et al., 1999) as well as pollen data from Wonderkrater and Rietvlei Dam (Scott et al., 2012) in southeastern Africa.

5.2.2 ∼ 950–650 cal yr BP – Medieval Climate Anomaly

At ∼ 950 cal yr BP a shift occurred to slightly lower SSTs (Fig. 4d) in the study area. At the same time, fluvial deposition became more dominant in the record: there is a strong increase in terrigenous input described by a higher index of fluvial input based on microfossil composition, a higher Fe content, an increased BIT (from ∼ 0.1 to 0.3) as well as a 2-fold increase in clay and silt content (to 40–60 %) (Fig. 4a–c, f). This increase in terrigenous input may either indicate a decrease in Agulhas strength, an increase in sediment delivery via the Gouritz River or a combination of both. Simultaneously a slight shift (0.5 ‰) towards lower average $\delta^{13}C_{C_{31}}$ values in the sediment core can be observed. Heavier isotope ^{13}C is more depleted in C_3 plants, which are less adapted to aridity as opposed to C_4 (Collister et al., 1994). However, the observed shift is very minor and a change in vegetation type is unlikely to occur within the timescale in question. It is more probable that the $\delta^{13}C$ values became more depleted as the water-use efficiency of plants decreased in moister climatic conditions (Pate, 2001; Ehleringer and Cooper, 1988). In either case, $\delta^{13}C$ values of n-C_{31} alkanes exported from the catchment suggest a shift towards more humid conditions on land after 950 cal yr BP. At the same time, δD values of the leaf wax n-C_{31} alkane shift to −129 ‰ indicating deuterium-enriched precipitation during this time. This likely indicates a shift to lower-altitude source regions. Enriched $\delta D_{C_{31}}$ values would be an indication for plant material mainly derived from more vegetated lowlands as opposed to plant material derived from the upper catchment during major flood events (see Sect. 5.1.1). Within the error margin of our age model, the shift we see at ∼ 950 ± 120 cal yr BP towards a more humid lower Gouritz River catchment is a general eastern South African expression of the northern hemispheric trend termed Medieval Climate Anomaly (MCA) summarized by Tyson and Lindesay (1992), Tyson and Preston-Whyte (2000) and Nash et al. (2016). A large array of continental records document this humid period throughout the South African summer rainfall zone (SRZ) (Talma and Vogel, 1992; Holmgren et al., 1999; Thomas and Shaw, 2002) as well as Wonderwerk Cave (Brook et al., 2015), Braamhoek Wetland, Free State (Norström et al., 2009, 2014), Lake Eteza, coastal KwaZulu-Natal (Neumann et al., 2010), Lake Sibaya, KwaZulu-Natal (Stager et al., 2013), Blydefontein Basin, Kikvorsberge (Scott et al., 2005), Katbakkies Pass, Swartruggens Mountains, southwestern Cape (Chase et al., 2015) and northeastern South African baobab trees (Woodborne et al., 2015). The few existing records of the YRZ record similar trends; a continuous rise in precipitation was found in $\delta^{15}N$ of hyrax middens at Seweweekspoort (Chase et al., 2013) and more evidently in the indirect (TOC-based) humidity record at Groenvlei – a Wilderness lake (Wündsch et al., 2016) (Fig. 4h–i). In contrast to the large array of available continental datasets, marine records are rare. The only SST record published for the area (Cohen and Tyson, 1995) does not include data for the time period in question. However, it does provide a conceptual model of ocean–atmosphere interplay to be tested (see Fig. 6). The authors postulate a periodically strengthened and more southerly South Indian Ocean anticyclone and South Atlantic anticyclone having an onshore as well as an offshore effect: (1) reinforcing the tropical easterly influence causing extended warm wet spells in the South African summer rainfall zone and (2) increasing the frequency of eastward ridging highs and, thus, alongshore winds driving the coastal upwelling on the eastern Agulhas Bank. Additionally, shelf-edge upwelling becomes more frequent when the strong South Indian Ocean anticyclone increases the Agulhas volume transport. The decrease in SSTs recorded in GeoB18308-1 for the in-

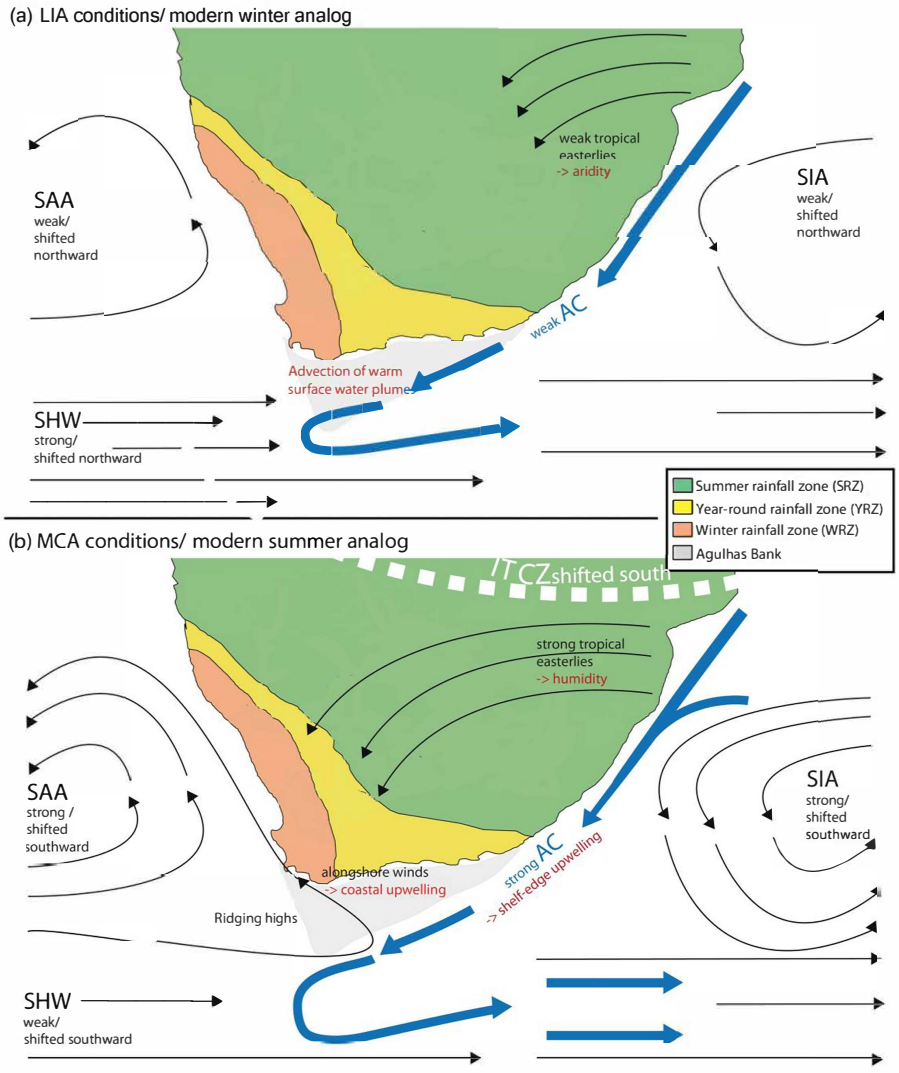

Figure 6. Conceptual model after Cohen and Tyson (1995) depicting the recorded response (in red) to shifts in atmospheric (indicated in black) and oceanic (in blue) circulation patterns during the LIA **(a)** and MCA **(b)**. Abbreviations: SIA (South Indian anticyclone), SAA (South Atlantic anticyclone), SHW (southern hemispheric westerlies), AC (Agulhas Current), LIA (Little Ice Age), MCA (Medieval Climate Anomaly), and ITCZ (Intertropical Convergence Zone).

terval of increased humidity in the Gouritz River catchment inferred in this study for the time interval of the Medieval Climate Anomaly serves as data to validate the conceptual model by Cohen and Tyson (1995) for which thus far no Medieval Climate Anomaly evidence by SST data had been available.

5.2.3 Conditions after ~650 cal yr BP – Little Ice Age and beyond

Continuous sedimentation at the core site was interrupted at ~650 cal yr BP. One or more erosive event deposits are inferred from the sedimentology (erosive contact at ~60–70 cm; fine sand with intercalated organic layers and lumps from ~30 to 60 cm) and an age reversal indicated by the two radiocarbon dates in this interval (~1466 cal yr BP at a depth of 31 cm ~640 cal yr BP at a depth of 60 cm; Fig. 3; Table 1). Due to the discontinuous nature of the deposition we are only able to curtail the timeframe of deposition to having taken place between ~650 cal yr BP (the youngest age in the event deposit) and a post-bomb date ~13.5 cm above the event deposit. From the redeposited sediment package three samples have been analyzed for organic geochemistry (see Table 3). The average values over the possible timeframe of deposition is plotted in Fig. 5. The high BIT (~0.7) indicates that the redeposited package can be characterized as reworked soil material. The averaged $\delta D_{C_{31}}$ signature of ~ −135 ‰ is comparable to that of Gouritz River paleoflood deposits described in Sect. 5.1.1. We therefore suggest that the origin of

the event-deposited material in core GeoB18308-1 is similar to the origin of these terrestrial paleoflood deposits, i.e., the upper parts of the Gouritz catchment (see Sect. 5.1.1). The shift in $\delta^{13}C_{C_{31}}$ towards slightly more depleted values in the event-deposited material in core GeoB18308-1 (average in the redeposited unit: $\sim -28\,‰$ VPDB) furthermore indicates that the n-C_{31} alkanes contained in the event deposit were produced by plants under less water stress (see Collister et al., 1994; Ehleringer and Cooper, 1988) than those deposited before ~ 650 cal yr BP. We therefore infer an increase in upper catchment rainfall inducing floods for the time period of the event deposit(s) (~ 300–650 cal yr BP). This roughly falls into the timeframe of the Little Ice Age (LIA) recorded as humid phase throughout the South African winter rainfall zone (Meadows et al., 1996; Benito et al., 2011; Stager et al., 2012; Weldeab et al., 2013). Most regional studies associate this increase in rainfall with a northward shift of the SHW (Tyson and Preston-Whyte, 2000; Chase and Meadows, 2007). A global study using high-resolution records (Lechleitner et al., 2017) also documents a southward shift of the ITCZ during the LIA interval; however, no data from the southern hemispheric midlatitudes are included and we suggest that the effects of this shifts are limited to locations north of our study site. In the uppermost Gouritz catchment (Seweweekspoort site) a major SHW-sourced rainfall regime has been documented (Chase et al., 2015). Desmet and Cowling (1999) indicate that despite the general summer rainfall zone regime in the Gouritz catchment, the SHW supplies additional rainfall in extreme events. We suggest that an increase in these extreme SHW-sourced rainfall events produced large floods during the LIA (~ 300–650 cal yr BP). After ~ 650 cal yr BP continuous sedimentation is re-established with sediment properties returning to pre-hiatus conditions. The return to "normal conditions" recorded at the GeoB18308-1 site after the LIA time interval (i.e., after ~ 300 cal yr BP) does not indicate any recent major Gouritz River flood events (e.g., the 1983 mega-flood documented by Damm and Hagedorn, 2010), underlining the magnitude of the LIA events.

6 Conclusions

The unique position of the core site directly offshore of the Gouritz River mouth at a central location on the South African south coast allows for a combined analysis of variability in marine processes as well as terrestrial input at a high temporal resolution. In order to reliably reconstruct terrestrial climatic change from an offshore record, measurements were performed down-core as well as on material from the Gouritz River catchment for ground truthing in a source to sink approach. Samples from the river and its flood deposits reveal that the sediments at our core site predominantly originate from the Gouritz River catchment. Furthermore, they indicate that paleoflood deposits are sourced from heavy rainfall events in the highlands, whereas soil formation processes are often linked to regular rainfall in the lowlands. The GeoB18308-1 sediment sequence records stable conditions on land and offshore prior to the Medieval Climate Anomaly (~ 950–650 cal yr BP), which in turn has been interpreted as a humid interval in the (lowland) regions of the Gouritz River catchment. The subsequent Little Ice Age (~ 300–650 cal yr BP) interval is characterized by major flood events attributed to (SHW) storm tracks influencing the upper catchment area. These paleoclimatic reconstructions correspond to available continental records for the region. This first regional SST dataset for the 2400–650 cal yr BP timeframe allows us to test the conceptual model of oceanic–atmospheric interplay (Cohen and Tyson, 1995) during short-term late Holocene climatic anomalies. In accordance with this model (see Fig. 6), our results indicate that variability in South Indian Ocean anticyclone location and strength drives both tropical easterly influence on South African summer rainfall zone climate and coastal upwelling on the eastern Agulhas Bank. During a poleward displacement and strengthening of the SIA (e.g., MCA situation) the stronger easterly (alongshore) winds cause the coastal upwelling, which is common during summer on the eastern Agulhas Bank, to become more frequent.

Data availability. Data used for this study are available at https://doi.pangaea.de/10.1594/PANGAEA.875943 (Hahn et al., 2017).

The Supplement related to this article is available online at https://doi.org/10.5194/cp-13-649-2017-supplement.

Competing interests. The authors declare that they have no conflict of interest.

Acknowledgements. This work was financially supported by the Bundesministerium für Bildung und Forschung (BMBF, Germany) within the project "Regional Archives for Integrated Investigations (RAiN)". We also thank the captain, crew and scientists of the *METEOR* M102 cruise for facilitating the recovery of the studied material and Christine Thies for her assistance in ECT fieldwork. This study would not have been possible without the support of MARUM. Thanks to all RAiN members as well as the reviewers and editor of this paper for critical discussion and helpful advice for our work progress.

The article processing charges for this open-access publication were covered by the University of Bremen.

Edited by: H. Bostock
Reviewed by: two anonymous referees

References

Andò, S. and Garzanti, E.: Raman spectroscopy in heavy-mineral studies, in: Sediment Provenance Studies in Hydrocarbon Exploration and Production, Geological Society, London, Special Publications, 386, 2013.

Andò, S., Garzanti, E., Padoan, M., and Limonta, M.: Corrosion of heavy minerals during weathering and diagenesis: a catalogue for optical analysis, Sediment. Geol., 280, 165–178, 2012.

Beckley, L. E.: Sea-surface temperature variability around Cape Recife, South Africa, South Afr. J. Sci., 79, 436–438, 1983.

Benito, G., Thorndycraft, V. R., Rico, M. T., Sanchez-Moya, Y., Sopena, A., Botero, B. A., Machado, M. J., Davis, M., and Perez-Gonzalez, A.: Hydrological response of a dryland ephemeral river to southern African climatic variability during the last millennium, Quaternary Res., 75, 471–482, https://doi.org/10.1016/j.yqres.2011.01.004, 2011.

Benson, R. H. and Maddocks, R. F.: Recent Ostracodes of Knysna Estuary, Cape Province, Union of South Africa, The University of Kansas Paleontological Contributions, Arthropoda, 5, 1–39, 1964.

Birch, G.: Nearshore Quaternary Sedimentation off the South Coast of South Africa, Joint Geological Survey, University of Cape Town, Technical Report 11, 127–146, 1978.

Blaauw, M. and Christen, J. A.: Flexible paleoclimate age-depth models using an autoregressive gamma process, Bayesian. Anal., 6, 457–474, https://doi.org/10.1214/ba/1339616472, 2011.

Boom, A., Carr, A. S., Chase, B. M., Grimes, H. L., and Meadows, M. E.: Leaf wax n-alkanes and δ13C values of CAM plants from arid southwest Africa, Org. Geochem., 67, 99–102, https://doi.org/10.1016/j.orggeochem.2013.12.005, 2014.

Bray, E. E. and Evans, E. D.: Distribution of n-paraffins as a clue to recognition of source beds, Geochim. Cosmochim. Acta, 22, 2–15, https://doi.org/10.1016/0016-7037(61)90069-2, 1961.

Brook, G. A., Railsback, L. B., Scott, L., Voarintsoa, N. R. G., and Liang, F.: Late Holocene stalagmite and tufa climate records for Wonderwerk Cave: Relationships between archaeology and climate in southern Africa, African Archaeological Review, 32, 669–700, 2015.

Carr, A. S.: Late Quaternary palaeohydrology and palaeoecology of southern Africa revealed by lipid biomarker analysis of rock hyrax middens, Quat. Int., 279, 81, 2012.

Carr, A. S., Boom, A., Grimes, H. L., Chase, B. M., Meadows, M. E., and Harris, A.: Leaf wax n-alkane distributions in arid zone South African flora: Environmental controls, chemotaxonomy and palaeoecological implications, Org. Geochem., 67, 72–84, https://doi.org/10.1144/SP411.11, 2014.

Cawthra, H. C.: The marine geology of Mossel Bay, Ph.D. thesis, University of Cape Town, 283, 2014.

Cawthra, H. C., Compton, J. S., Fisher, E. C., Machutchon, M. R., and Marean, C. W.: Submerged shorelines and landscape features offshore of Mossel Bay, South Africa, in: Geology and Archaeology: Submerged Landscapes of the Continental Shelf, Geol. Soc. Spec. Publ., 411, London, https://doi.org/10.1144/SP411.11, 2015.

Chase, B. M. and Meadows, M. E.: Late Quaternary dynamics of southern Africa's winter rainfall zone, Earth-Sci. Rev., 84, 103–138, https://doi.org/10.1016/j.earscirev.2007.06.002, 2007.

Chase, B. M., Meadows, M. E., Scott, L., Thomas, D. S. G., Marais, E., Sealy, J., and Reimer, P. J.: A record of rapid Holocene climate change preserved in hyrax middens from southwestern Africa, Geology, 37, 703–706, https://doi.org/10.1130/G30053A.1, 2009.

Chase, B. M., Meadows, M. E., Carr, A. S., and Reimer, P. J.: Evidence for progressive Holocene aridification in southern Africa recorded in Namibian hyrax middens: Implications for African Monsoon dynamics and the African Humid Period, Quat. Res., 74, 36–45, https://doi.org/10.1016/j.yqres.2010.04.006, 2010.

Chase, B. M., Quick, L. J., Meadows, M. E., Scott, L., Thomas, D. S. G., and Reimer, P. J.: Late glacial interhemispheric climate dynamics revealed in South African hyrax middens, Geology, 39, 19–22, https://doi.org/10.1130/G31129.1, 2011.

Chase, B. M., Boom, A., Carr, A. S., Meadows, M. E., and Reimer, P. J.: Holocene climate change in southernmost South Africa: rock hyrax middens record shifts in the southern westerlies, Quat. Sci. Rev., 82, 199–205, https://doi.org/10.1016/j.quascirev.2013.10.018, 2013.

Chase, B. M., Lim, S., Chevalier, M., Boom, A., Carr, A. S., Meadows, M. E., and Reimer, P. J.: Influence of tropical easterlies in southern Africa's winter rainfall zone during the Holocene, Quat. Sci. Rev., 107, 138–148, 2015.

Chevalier, M. and Chase, B. M.: Southeast African records reveal a coherent shift from high- to low-latitude forcing mechanisms along the east African margin across last glacial–interglacial transition, Quat. Sci. Rev., 125, 117–130, https://doi.org/10.1016/j.quascirev.2015.07.009, 2015.

Cohen, A. and Tyson, P. D.: Sea-surface temperature fluctuations during the Holocene off the south coast of Africa: implications for terrestrial climate and rainfall, The Holocene, 5, 304–312, 1995.

Collister, J. W., Rieley, G., Stern, B., Eglinton, G., and Fry, B.: Compound-specific δ 13C analyses of leaf lipids from plants with differing carbon dioxide metabolisms, Org. Geochem., 21, 619–627, https://doi.org/10.1016/0146-6380(94)90008-6, 1994.

Compton, J. S.: The mid-Holocene sea-level highstand at Bogenfels Pan on the southwest coast of Namibia, Quat. Res., 66, 303–310, 2006.

Cowling, R. M., Richardson, D. M., and Pierce, S. M.: Vegetation of southern Africa, Cambridge University Press, 2004.

Damm, B. and Hagedorn, J.: Holocene floodplain formation in the southern Cape region, South Africa, Geomorphology, 122, 213–222, 2010.

Daniau, A.-L., Sánchez-Goñi, M. F., Martinez, P., Urrego, D. H., Bout-Roumazeilles, V., Desprat, S., and Marlon, J. R.: Orbital-scale climate forcing of grassland burning in southern Africa, P. Natl. Acad. Sci., 110, 5069–5073, https://doi.org/10.1073/pnas.1214292110, 2013.

Desmet, P. G. and Cowling, R. M.: The climate of the Karoo–a functional approach, Karoo Ecol. Patterns Process, Camb. Univ. Press, Camb, 3–16, 1999.

Dewar, G., Reimer, P. J., Sealy, J., and Woodborne, S.: Late-Holocene marine radiocarbon reservoir correction (Delta R) for the west coast of South Africa, Holocene, 22, 1481–1489, 2012.

Dingle, R. V.: Quaternary ostracods from the continental margin off south-western Africa. Part I Dominant Taxa, Ann. S. Afr. Mus., 102, 1–89, 1992.

Dingle, R. V.: Quaternary ostracods from the continental margin off south-western Africa. Part II. Minor Taxa, Ann. S. Afr. Mus., 103, 1–165, 1993.

Dingle, R. V.: Quaternary ostracods from the continental margin off south-western Africa. Part III. Oceanographical and Sedimentary Environments, Ann. S. Afr. Mus., 103, 383–441, 1994.

Dingle, R. V. and Honigstein, A.: Ostracoda from Quaternary coastal sequences in the south-western Cape, Ann. S. Afr. Mus., 104, 63–114, 1994.

Duncan, R. A., Hooper, P. R., Rehacek, J., Marsh, J. S., and Duncan, A. R.: The timing and duration of the Karoo igneous event, southern Gondwana, J. Geophys. Res., 102, 18127–18138, 1997.

Dupont, L. M., Caley, T., Kim, J.-H., Castañeda, I., Malaizé, B., and Giraudeau, J.: Glacial-interglacial vegetation dynamics in South Eastern Africa coupled to sea surface temperature variations in the Western Indian Ocean, Clim. Past, 7, 1209–1224, https://doi.org/10.5194/cp-7-1209-2011, 2011.

Ehleringer, J. R. and Cooper, T. A.: Correlations between carbon isotope ratio and microhabitat of desert plants, Oecologia, 76, 562–566, 1988.

Gagosian, R. B. and Peltzer, E. T.: The importance of atmospheric input of terrestrial organic material to deep-sea sediments, Org. Geochem., 10, 661–669, 1986.

Galehouse, J. S.: Point counting, in: Procedures in sedimentary petrology, Wiley, New York, 385–407, 1971.

Goldblatt, P. and Manning, J. C.: Plant diversity of the Cape region of southern Africa, Ann. Mo. Bot. Gard., 89, 281–302, 2002.

Gonfiantini, R., Roche, M.-A., Olivry, J.-C., Fontes, J.-C., and Zuppi, G. M.: The altitude effect on the isotopic composition of tropical rains, Chemical Geology, 181, 147–167, https://doi.org/10.1016/S0009-2541(01)00279-0, 2001.

Govin, A., Varma, V., and Prange, M.: Astronomically forced variations in western African rainfall (21° N–20° S) during the Last Interglacial period, Geophys. Res. Lett., 41, 2117–2125, https://doi.org/10.1002/2013GL058999, 2014.

Hahn, A., Schefuß, E., Andó, S., Cawthra, H., Frenzel, P., Kugel, M., Meschner, S., Mollenhauer, G., and Zabel, M.: Supplementary material to: Linking catchment hydrology and ocean circulation in Late Holocene southernmost Africa, available at: https://doi.pangaea.de/10.1594/PANGAEA.875943, 2017.

Hammer, O., David, A. T., and Ryan, P. D.: Past Paleontological Statistics Software Package for Education and Data Analysis, Palaeontol. Electronica, 4, 2001.

Herrmann, N., Boom, A., Carr, A. S., Chase, B. M., Granger, R., Hahn, A., Zabel, M., and Schefuß, E.: Sources, transport and deposition of terrestrial organic material: A case study from southwestern Africa, Quat. Sci. Rev., 149, 215–229, https://doi.org/10.1016/j.quascirev.2016.07.028, 2016.

Hogg, A. G., Hua, Q., Blackwell, P. G., Niu, M., Buck, C. E., Guilderson, T. P., Heaton, T. J., Palmer, J. G., Reimer, P. J., Reimer, R. W., Turney, C. S. M., and Zimmerman, S. R. H.: SHCal13 Southern Hemisphere Calibration, 0–50,000 Years cal BP, Radiocarbon, 55, 1–15 2013.

Holmgren, K., Karlén, W., Lauritzen, S. E., Lee-Thorp, J. A., Partridge, T. C., Piketh, S., and Tyson, P. D.: A 3000-year high-resolution stalagmite based record of palaeoclimate for north-eastern South Africa, The Holocene, 9, 295–309, 1999.

Hopmans, E. C., Schouten, S., Pancost, R. D., van der Meer, M. T., and Sinninghe Damsté, J. S.: Analysis of intact tetraether lipids in archaeal cell material and sediments by high performance liquid chromatography/atmospheric pressure chemical ionization mass spectrometry, Rapid Commun. Mass Spectrom., 14, 585–589, 2000.

Hopmans, E. C., Weijers, J. W., Schefuß, E., Herfort, L., Damsté, J. S. S., and Schouten, S.: A novel proxy for terrestrial organic matter in sediments based on branched and isoprenoid tetraether lipids, Earth Planet. Sci. Lett., 224, 107–116, 2004.

Hutchings, L., Pitcher, G. C., Probyn, T. A., and Bailey, G. W.: The chemical and biological consequences of coastal upwelling, Environmental Sciences Research Report Es, 18, 65–82, 1995.

Johnson, M. R., van Vuuren, C. J., Visser, J. N. J., Cole, D. I., De Wickens, V., Christie, A. D. M., Roberts, D. L., and Brandl, G.: Sedimentary rocks of the Karoo Supergroup, in: The Geology of South Africa, Geological Society of South Africa, 461–501, 2006.

Jury, M. R., Valentine, H. R., and Lutjeharms, J. R. E.: Influence of the Agulhas Current on Summer Rainfall along the Southeast Coast of South Africa, J. Appl. Meteorol., 32, 1282–1287, 1993.

Kim, J.-H., van der Meer, J., Schouten, S., Helmke, P., Willmott, V., and Sangiorgi, F.: New indices and calibrations derived from the distribution of crenarchaeal isoprenoid tetraether lipids: Implications for past sea surface temperature reconstructions, Geochim. Cosmochim.Acta, 74, 4639–4654, 2010.

Lechleitner, F. A., Breitenbach, S. F., Rehfeld, K., Ridley, H. E., Asmerom, Y., Prufer, K. M., Marwan, N., Goswami, B., Kennett, D. J., and Aquino, V. V.: Tropical rainfall over the last two millennia: evidence for a low-latitude hydrologic seesaw, Scientific Reports, 7, 45809, https://doi.org/10.1038/srep45809, 2017.

Le Maitre, D., Colvin, C., and Maherry, A.: Water resources in the Klein Karoo: the challenge of sustainable development in a water-scarce area, South Afr. J. Sci., 105, 39–48, 2009.

Locarini, R. A., Mishonov, A. V., Antonov, J. I., Boyer, T. P., Garcia, H. E., Baranova, O. K., Zweng, M. M., Paver, C. R., Reagan, J. R., Johnson, D. R., Hamilton, M., and Seidov, D.: World Ocean Atlas 2013, Volume 1: Temperature, NOAA Atlas NESDIS, 73, 2013.

Lowry, F. M. D.: Foraminiferal thanatocoenoses from the continental shelf of Southern Africa, Ph.D. Thesis, Department of Geological Sciences, University College London, 1–443, 1987.

Lutjeharms, J. R. E. and van Ballegooyen, R. C.: The retroflection of the Agulhas Current, J. Phys. Oceanogr., 18, 1570–1583, 1988.

Lutjeharms, J. R. E., Monteiro, P. M. S., Tyson, P. D., and Obura, D.: The oceans around southern Africa and regional effects of global change, S. Afr. J. Sci., 97, 119–130, 2001.

Lyle, M., Lyle, A. O., Gorgas, T., Holbourn, A., Westerhold, T., Hathorne, E., Kimoto, K., and Yamamoto, S.: Data report: raw and normalized elemental data along the Site U1338 splice from X-ray fluorescence scanning 1, Proc. Integr. Ocean. Drill. Program, 320(320/321), 2012.

Martens, K., Davies, B. R., Baxter, A. J., and Meadows, M. E.: A contribution to the taxonomy and ecology of the Ostracoda (Crustacea) from Verlorenvlei (Western Cape, South Africa), S. Afr. J. Zool., 31, 23–36, 1996.

Marzin, C. and Braconnot, P.: Variations of Indian and African monsoons induced by insolation changes at 6 and 9.5 kyr BP, Clim. Dyn., 33, 215–231, https://doi.org/10.1007/s00382-009-0538-3, 2009.

Meadows, M. E. and Osmal, A.: Chronology, sedimentology and geochemistry of sediments at Verlorenvlei (Western Cape Province, South Africa) as evidence of anthropogenicallyinduced land degradation, Z. Geomorph. Supp. Bd., 107, 45–62, 1996.

Milani, E. J. and De Wit, M. J.: Correlations between the classic Paraná and Cape–Karoo sequences of South America and southern Africa and their basin infills flanking the Gondwanides: du Toit revisited, Geol. Soc., London, Spec. Publ., 294, 319–342, 2008.

Mucina, L. and Rutherford, M. C.: The Vegetation of South Africa, Lesotho and Swaziland, South African National Biodiversity Institute, 2006

Nash, D. J., De Cort, G., Chase, B. M., Verschuren, D., Nicholson, S. E., Shanahan, T. M., Asrat, A., Lézine, A.-M., and Grab, S. W.: African hydroclimatic variability during the last 2000 years, Quat. Sci. Rev., 154, 1–22, https://doi.org/10.1016/j.quascirev.2016.10.012, 2016.

Neumann, F. H., Scott, L., Bousman, C. B., and van As, L. A.: Holocene sequence of vegetation change at Lake Eteza, coastal KwaZulu-Natal, South Africa, Rev. Palaeobot. Palynol., 162, 39–53, https://doi.org/10.1016/j.revpalbo.2010.05.001, 2010.

Newton, A. R., Shone, R. W., and Booth, P. W. K.: The Cape Fold Belt, in: The Geology of South Africa, Geological Society of South Africa, Johannesburg/Council for Geoscience Pretoria, 521–531, 2006.

Niang, I., Ruppel, O. C., Abdrabo, M. A., Essel, A., Lennard, C., Padgham, J., and Urquhart, P.: Africa, in: Climate Change: Impacts, Adaptation, and Vulnerability. Part B: Regional Aspects, Contribution of Working Group II to the Fifth Assessment Report of the Intergovernmental Panel on Climate Change, Cambridge University Press, Cambridge, United Kingdom and New York, NY, USA, 1199–1265, 2014.

Norström, E., Scott, L., Partridge, T., Risberg, J., and Holmgren, K.: Reconstruction of environmental and climate changes at Braamhoek wetland, eastern escarpment South Africa, during the last 16,000 years with emphasis on the Pleistocene–Holocene transition, Palaeogeogr. Palaeoclimatol. Palaeoecol., 271, 240–258, 2009.

Norström, E., Neumann, F. H., Scott, L., Smittenberg, R. H., Holmstrand, H., Lundqvist, S., Snowball, I., Sundqvist, H. S., Risberg, J., and Bamford, M.: Late Quaternary vegetation dynamics and hydro-climate in the Drakensberg, South Africa, Quat. Sci. Rev., 105, 48–65, 2014.

Pate, J. S.: Carbon isotope discrimination and plant water-use efficiency: case scenarios for C3 plants, in: Stable Isotope Techniques in the Study of Biological Processes and Functioning of Ecosystems, Kluwer Academic Publishers, Dordrecht, 19–37, 2001

Ramsay, P. J. and Cooper, J. A. G.: Late Quaternary Sea-Level Change in South Africa, Quatern. Res., 57, 82–90, 2002.

Reimer, P. J., Bard, E., Bayliss, A., Beck, J. W., Blackwell, P. G., Bronk- Ramsey, C., Buck, C. E., Cheng, H., Edwards, R. L., and Friedrich, M.: IntCal13 and Marine13 radiocarbon age calibration curves 0–50,000 years cal BP, Radiocarbon, 55, 1869–1887, 2013.

Rommerskirchen, F., Plader, A., Eglinton, G., Chikaraishi, Y., and Rullkötter, J.: Chemotaxonomic significance of distribution and stable carbon isotopic composition of long-chain alkanes and alkan-1-ols in C4 grass waxes, Org. Geochem., 37, 1303–1332, https://doi.org/10.1016/j.orggeochem.2005.12.013, 2006.

Rouault, M., Florenchie, P., Fauchereau, N., and Reason, C. J. C.: South East tropical Atlantic warm events and southern African rainfall, Geophys. Res. Lett., 30, 8009, https://doi.org/10.1029/2002gl014840, 2003.

Rozendaal, A., Gresse, P. G., Scheepers, R., and Le Roux, J. P.: Neoproterozoic to Early Cambrian crustal evolution of the Pan-African Saldania Belt, South Africa, Precambrian Res., 97, 303–323, 1999.

Rundel, P. W., Esler, K. J., and Cowling, R. M.: Ecological and phylogenetic patterns of carbon isotope discrimination in the winter-rainfall flora of the Richtersveld, South Africa, Plant Ecol., 142, 133–148, https://doi.org/10.1023/A:1009878429455, 1999.

Schefuß, E., Kuhlmann, H., Mollenhauer, G., Prange, M., and Pätzold, J.: Forcing of wet phases in southeast Africa over the past 17,000 years, Nature, 480, 509–512, https://doi.org/10.1038/nature10685, 2011.

Schmidt-Sinns, J.: Rezente benthische Foraminiferen im Bereich des Benguelastroms, Südwestafrika – Verbreitungsmuster und ihre steuernden Faktoren, Doctoral dissertation, Universitäts- und Landesbibliothek Bonn, 1–261, 2008.

Schouten, S., Hopmans, E. C., Schefuß, E., and Sinninghe Damsté, J. S.: Distributional variations in marine crenarchaeotal membrane lipids: a new tool for reconstructing ancient sea water temperatures, Earth Planet. Sci. Lett., 204, 265–274, 2002.

Schumann, E. H., Perrins, L. A., and Hunter, I. T.: Upwelling along the south coast of the Cape Province, South Africa, S. Afr. J. Sci., 78, 238–242, 1982.

Scott, L., Bousman, C. B., and Nyakale, M.: Holocene pollen from swamp, cave and hyrax dung deposits at Blydefontein (Kikvorsberge), Karoo, South Africa, Quaternary International, 129, 49–59, https://doi.org/10.1016/j.quaint.2004.04.006, 2005.

Scott, L., Neumann, F. H., Brook, G. A., Bousman, C. B., Norström, E., and Metwally, A. A.: Terrestrial fossil-pollen evidence of climate change during the last 26 thousand years in Southern Africa, Quat. Sci. Rev., 32, 100–118, 2012.

Sessions, A. L., Burgoyne, T. W., Schimmelmann, A., and Hayes, J. M.: Fractionation of hydrogen isotopes in lipid biosynthesis, Organic Geochemistry, 30, 1193–1200, https://doi.org/10.1016/S0146-6380(99)00094-7, 1999.

Simon, M. H., Ziegler, M., Bosmans, J., Barker, S., Reason, C. J. C., and Hall,I. R.: Eastern South African hydroclimate over the past 270,000 years, Scientific Reports, 5, 18153, https://doi.org/10.1038/srep18153, 2015.

Stager, J. C., Mayewski, P. A., White, J., Chase, B. M., Neumann, F. H., Meadows, M. E., King, C. D., and Dixon, D. A.: Precipitation variability in the winter rainfall zone of South Africa during the last 1400 yr linked to the austral westerlies, Clim. Past, 8, 877–887, https://doi.org/10.5194/cp-8-877-2012, 2012.

Stager, J. C., Ryves, D. B., King, C., Madson, J., Hazzard, M., Neumann, F. H., and Maud, R.: Late Holocene precipitation variability in the summer rainfall region of South Africa, Quat. Sci. Rev., 67, 105–120, https://doi.org/10.1016/j.quascirev.2013.01.022, 2013.

Talma, A. and Vogel, J. C.: Late Quaternary paleotemperatures derived from a speleothem from Cango caves, Cape province, South Africa, Quaternary Res. 37, 203–213, 1992.

Thamm, A. G. and Johnson, M. R.: The Cape Supergroup, in: The Geology of South Africa, Geological Society of South Africa, Johannesburg/Council for Geoscience Pretoria, 443–461, 2006.

Thomas, D. S. and Shaw, P. A.: Late Quaternary environmental change in central southern Africa: new data, synthesis, issues and prospects, Quaternary Sci. Rev., 21, 783–797, 2002.

Tierney, J. E., Russell, J. M., Huang, Y., Damsté, J. S. S., Hopmans, E. C., and Cohen, A. S.: Northern Hemisphere Controls on Tropical Southeast African Climate During the Past 60,000 Years, Science, 322, 252–255, 2008.

Truc, L., Chevalier, M., Favier, C., Cheddadi, R., Meadows, M. E., Scott, L., Carr, A. S., Smith, G. F., and Chase, B. M.: Quantification of climate change for the last 20,000 years from Wonderkrater, South Africa: implications for the long-term dynamics of the Intertropical Convergence Zone, Palaeogeogr. Palaeoclimatol. Palaeoecol., 386, 575–587, 2013.

Tyson, P. D. and Lindesay, J.: The climate of the last 2000 years in southern Africa, The Holocene, 2, 271–278, 1992.

Tyson, P. D. and Preston-Whyte, R. A.: Weather and climate of southern Africa, Oxford University Press, 2000.

Vogel, J. C., Fuls, A., and Ellis, R. P.: Geographical distribution of Kranz grasses in South Africa, South Afr. J. Sci., 1978.

Vogts, A., Moossen, H., Rommerskirchen, F., and Rullkötter, J.: Distribution patterns and stable carbon isotopic composition of alkanes and alkan-1-ols from plant waxes of African rain forest and savanna species, Org. Geochem., 40, 1037–1054, 2009.

Weijers, J. W. H., Schefuß, E., Kim, J. H., Sinninghe Damsté, J. S., and Schouten, S.: Constraints on the sources of branched tetraether membrane lipids in distal marine sediments, Org. Geochem., 72, 14–22, https://doi.org/10.1016/j.orggeochem.2014.04.011, 2014.

Weldeab, S., Stuut, J.-B. W., Schneider, R. R., and Siebel, W.: Holocene climate variability in the winter rainfall zone of South Africa, Clim. Past, 9, 2347–2364, https://doi.org/10.5194/cp-9-2347-2013, 2013.

Woodborne, S., Hall, G., Robertson, I., Patrut, A., Rouault, M., Loader, N. J., and Hofmeyr, M.: A 1000-Year Carbon Isotope Rainfall Proxy Record from South African Baobab Trees (< italic> Adansonia digitata< /italic> L.), PLoS ONE, 10, e0124202, https://doi.org/10.1371/journal.pone.0124202, 2015.

Wündsch, M., Haberzettl, T., Kirsten, K. L., Kasper, T., Zabel, M., Dietze, E., Baade, J., Daut, G., Meschner, S., Meadows, M. E., and Mäusbacher, R.: Sea level and climate change at the southern Cape coast, South Africa, during the past 4.2 kyr, Palaeogeogr. Palaeoclimatol. Palaeoecol., 446, 295–307, https://doi.org/10.1016/j.palaeo.2016.01.027, 2016.

Ziervogel, G., New, M., Archer van Garderen, E., Midgley, G., Taylor, A., Hamann, R., Stuart-Hill, S., Myers, J., and Warburton, M.:Climate change impacts and adaptation in South Africa, WIREs Clim Change, 5, 605–620, https://doi.org/10.1002/wcc.295, 2014,